

Article

The Atomistic Understanding of the Ice Recrystallization Inhibition Activity of Antifreeze Glycoproteins

Wentao Yang , Yucong Liao, Qi Shi and Zhaoru Sun *

School of Physical Science and Technology, ShanghaiTech University, Shanghai 201210, China

* Correspondence: sunzhr@shanghaitech.edu.cn

Abstract: As the most potent ice recrystallization inhibitors, antifreeze glycoproteins (AFGPs) have been extensively studied since their discovery. However, the molecular mechanism of how they inhibit ice growth remains controversial—notably, which group directly contributes to the binding of AFGPs to ice is hotly debated. Here, we use molecular dynamics simulations to investigate the atomistic details of the binding of AFGP8 to ice. We show that the binding of AFGP8 to ice can be divided into three cases: backbone dominant binding (BDB), disaccharide dominant binding (DDB) and weak binding (WB). Hydrogen-bonding and hydrophobic groups contribute equally to the binding of AFGP8 to ice and synergistically promote the binding. The $-\text{CH}_3$ groups promote the contacting of AFGP8 to ice via hydrophobic effect, and the hydrogen-bonding groups anchor AFGP8 to ice surfaces through direct hydrogen bonding with ice. Specially, we verify that the $-\text{CONH}$ -groups anchor the backbone of AFGP8 to ice by forming hydrogen bonds with ice surfaces while the $-\text{OH}$ groups not only anchor the disaccharide to ice but also slow down the dynamics of the surrounding water. In addition, we reveal that both the backbone and the disaccharide can bind to ice surfaces while the latter is more flexible, which also perturbs the hydrogen bond network of potential ice-like water molecules by swaying in the solution to further enhance its antifreeze activity. This work provides the atomistic details of the ice growth inhibition mechanism of AFGP8, which is helpful for the design of high-efficacy cryoprotectants.

Keywords: antifreeze; ice growth; antifreeze glycoproteins; ice recrystallization inhibition



Citation: Yang, W.; Liao, Y.; Shi, Q.; Sun, Z. The Atomistic Understanding of the Ice Recrystallization Inhibition Activity of Antifreeze Glycoproteins. *Crystals* **2023**, *13*, 405. <https://doi.org/10.3390/cryst13030405>

Academic Editor: José Gavira

Received: 13 February 2023

Revised: 23 February 2023

Accepted: 24 February 2023

Published: 26 February 2023



Copyright: © 2023 by the authors. Licensee MDPI, Basel, Switzerland. This article is an open access article distributed under the terms and conditions of the Creative Commons Attribution (CC BY) license (<https://creativecommons.org/licenses/by/4.0/>).

1. Introduction

Antifreeze proteins (AFPs) and antifreeze glycoproteins (AFGPs) allow organisms to survive in subzero habitats [1–5]. These natural proteins, as well as synthetic mimics, are of enormous interest for their use in biomedicine [6–11], the food industry [12–14] and engineering deicing [15–18]. Antifreeze glycoproteins have three macroscopic antifreeze properties resulting from their ice interactions: ice recrystallization inhibition (IRI) [19,20], thermal hysteresis (TH) [1,21] and dynamic ice shaping (DIS) [22–24]. The former (IRI) is of particular interest because this property is easier to mimic and central to application in cryopreservation [25–31]. This property is generally explained by an adsorption-inhibition mechanism in which the proteins recognize and bind to specific ice surfaces, thereby preventing macroscopic ice growth [32,33]. Antifreeze glycoproteins, composed with tripeptide repeats of alanine-alanine-threonine (Ala-Ala-Thr) in which the hydroxyl group of the Thr is glycosylated with β -D-galactosyl-(1,3)- α -N-acetyl-D-galactosamine (Figure 1a) [34–36], are the most potent IRI agents [37]. Antifreeze glycoproteins are classified as AFGP1 to AFGP8 based on the number of Ala-Ala-Thr repeat units, and some of Ala in the smaller AFGPs (AFGP7-8) may be substituted by Pro [36]. A series of experiments have indicated that AFGPs are preferentially adsorbed at the prismatic and pyramidal surfaces of ice to inhibit ice growth [37–41]. Despite the previous studies having reached a consensus that poly-L-proline type II (PPII) helix conformations (as shown in Figure 1b) play a crucial role

in the binding of AFGPs to ice [42–47], the molecular details of how AFGPs bind to ice remain largely elusive due to its high flexibility and complex components [9,48–50].

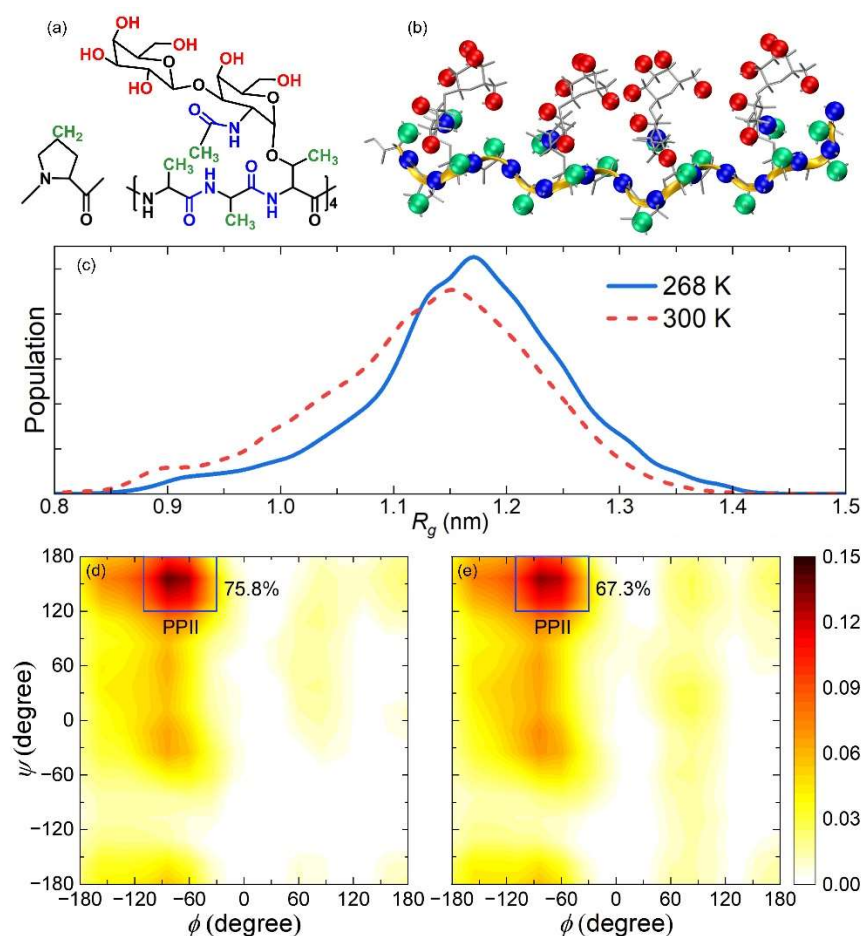


Figure 1. The Structure of AFGP8. (a) Sequence of AFGP8 is Ala-Ala-T*-Ala-Ala-T*-Pro-Ala-T*-Ala-Ala-T*-Pro-Ala, where T* denotes the glycosylated Thr. (b) The three-dimensional structure with PPII helix conformation of AFGP8, and the key groups, are heightened with the balls: methyl groups (green balls), amide groups (blue balls) and hydroxyl groups (red balls). (c) Distribution of the radius of gyration R_g of AFGP8 in solution at 268 K (solid blue line) and 300 K (dashed red line). Ramachandran plots of AFGP8 at 268 K (d) and 300 K (e). Darker colors represent the higher specific gravity of the secondary structures. The populations of PPII helix integrated inside the region heightened with a blue square are also shown.

Several scenarios have been proposed for the binding of AFGPs to ice. One is based on the direct interaction of the hydrogen-bonding groups of AFGPs to ice. Some experiments have substituted certain disaccharide moieties and illustrated that the disaccharide plays a significant role in the anti-freezing of AFGPs [37,51–54]. A 2D infrared spectroscopy study by Giubertoni et al. [47] indicated that AFGPs bind to ice through their disaccharide chains. Knight et al. [40] proposed a model where the hydrogen bonds formed between AFGP8 and the ice is vital for the irreversible binding of AFGP8. Moreover, a delicate experiment by Sun et al. [50] confirmed that all the hydroxyl (–OH) groups on the disaccharides are necessary for the unique antifreeze activity of AFGP8. A recent simulation study by Zhang et al. [55] showed that –OH groups can form hydrogen bonds with ice and promote the binding of AFGP8 to ice. In the study of other IRI agents, such as poly (vinyl)alcohol (PVA) [56–58] and nanogold modified with small molecules [59], hydrogen bonding has also been proved to be the dominant driving force for the binding of antifreeze agents to ice. Therefore, it is believed that hydrogen bonding is directly involved in the binding of AFGPs to ice.

This view, however, has been challenged since it is almost impossible to directly observe which part of AFGP binds to ice in experiments. Harding et al. [35] pointed out that the hydrogen bonding may not be as prevalent as hydrophobic effects for AF(G)Ps and the latter may dominate the binding of AFGPs to ice, but they did not prove it directly. Based on MD simulations, Mochizuki and Molinero [45] reported that AFGPs bind to ice via hydrophobic groups rather than the –OH groups of the disaccharides. The substitutional experiments by Tachibana et al. [60] have also shown that the methyl group of threonine is important for the unique antifreeze activity of AFGP8. Therefore, a systematical study of the specific roles of hydrogen-bonding and hydrophobic groups in the IRI activity of AFGP8 is still very necessary.

Here, we performed molecular dynamic (MD) simulations to elucidate the ice growth inhibition mechanism of AFGP8 (the smallest AFGP) by systematically investigating the roles of –CH₃, –CONH– and –OH groups of AFGP8 in the binding of AFGP8 to ice and the water dynamics of AFGP8 solutions. We find that the hydrogen-bonding (–CONH– or –OH) and hydrophobic (–CH₃) groups synergistically promote the binding of AFGP8 to ice. Specifically, the –CH₃ groups promote the contacting of AFGP8 to ice via hydrophobic effect, while the –CONH– groups anchor the backbone of AFGP8 to ice by forming hydrogen bonds with ice surfaces and the –OH groups anchor the disaccharide to ice through hydrogen bonding. In contrast to the backbone, which adsorbs on ice surfaces more easily due to its rigidity, the disaccharides exhibit dual roles due to their hydrophilicity and flexibility. Some of the disaccharides anchor to ice while the others destroy the hydrogen bond network of potential ice-like water molecules by swaying in the solution. Our results provide an important molecular guidance for the design of more efficient antifreeze agents that could be used for tissue cryopreservation and in other fields.

2. Methods

2.1. Molecular Dynamics Simulations

All the MD simulations and free energy calculations are carried out by GROMACS 2019.5 packages [61,62] using the all-atomistic OPLS-AA [63] force field and the TIP4P/Ice water model [64]. The melting temperature of ice Ih in this water model is 270 K [65], in very good agreement with the experimental value of 273.15 K. The Lennard-Jones, bond and angle parameters of C, H and O of CH₃CH₃, CH₃CONH₂ and CH₃OH for the free energy calculations are identical to corresponding groups of AFGP8, without partial charges. The Lennard-Jones parameters for cross-interactions are obtained through the combination rules: $\epsilon_{ij} = (\epsilon_{ii}\epsilon_{jj})^{1/2}$ and $\sigma_{ij} = (\sigma_{ii}\sigma_{jj})^{1/2}$. The cutoffs for the van der Waals and coulombic interactions are set to 1.2 nm. The long-range Coulombic interactions are evaluated with the particle-mesh Ewald algorithm. Equations of motion are integrated using leapfrog with a time step of 2 fs. The temperature T and pressure P for production runs are controlled with the Nosé–Hoover thermostat [66,67] and Parrinello–Rahman barostat [68], with time constants of 0.2 and 1.0 ps, respectively. Periodic boundary conditions are applied in three directions. The pressure is set to 1 atm in all NPT-MD simulations.

To investigate the impact of AFGP8 on ice growth when exposed to an advancing ice front on the prism surface of ice Ih, we build the ice slab system, which contains one AFGP8 molecule, and then solvated by ~10000 water molecules, as experiments have reported that AFGP8 exhibits TH activity even at concentrations below 20 mM [69]. The simulation box is set to 6.35 × 6.64 × 10.00 nm³. Two layers of ice Ih (1008 molecules) constrained by a harmonic potential with force constant of 1000 kJ mol⁻¹ nm⁻² are generated by the Genice program [70] with the density of 0.909 g cm⁻³. The center of mass of AFGP8 is initially placed approximately 1.1 nm above the ice surfaces. We perform more than a dozen independent simulations with different backbone orientations parallel to the ice surface. First, the energy minimization is conducted using the steepest descent method with the force tolerance of 1000 kJ mol⁻¹ nm⁻¹. Then, a 500 ps NVT-MD simulation is performed for equilibration. Finally, a 1000 ns production NVT-MD run at 268 K is performed to monitor the IRI activity. We employ the CHILL+ algorithm [71] to identify one water molecule in ice

or liquid phase. Moreover, the water molecules with the distance less than 3.5 Å away from the ice molecules determined by the CHILL+ algorithm are also considered as ice molecules (~350 ice molecules in each frame), which has a better description for the advancing ice front. To estimate the interaction between the groups and ice, the $-\text{CH}_3$ group is treated as binding to ice surface if there are two ice molecules within 5.5 Å (first solvation shell) of it. The hydrogen bonds are identified with donor-acceptor distance less than 3.5 Å and hydrogen-donor-acceptor angle less than 30° [72].

2.2. Conformation Analysis

We perform the replica exchange molecular dynamic (REMD) simulations [73] to enhance the conformational sampling for AFGP8 in solution. We put an AFGP8 with the arbitrary initial conformation into a box with ~4500 water molecules. The system is energy-minimized and equilibrated for 1 ns in NPT ensembles for each replica. We execute REMD simulation in NPT ensemble for 400 ns in which 48 replicas are prepared by REMD-temperature-generator [74] in the temperature range of 268–398 K (i.e., 268.00, 270.39, 272.80, 275.24, 277.69, 280.15, 282.63, 285.12, 287.63, 290.16, 292.70, 295.26, 297.80, 300.00, 303.00, 305.69, 308.33, 311.00, 313.68, 316.37, 319.09, 321.83, 324.58, 327.35, 330.15, 332.96, 335.78, 338.63, 341.49, 344.38, 347.28, 350.21, 353.16, 356.12, 359.10, 362.10, 365.13, 368.17, 371.23, 374.31, 377.41, 380.53, 383.68, 386.84, 390.03, 393.24, 396.46, 398.00 K). The replicas are exchanged every 10 ps and the average exchange ratio between nearest neighbor temperatures is $26.6 \pm 6.0\%$. The radius of gyration (R_g) and the Ramachandran plots are computed from REMD trajectories.

2.3. Free Energies

The umbrella sampling approach [75,76] is adopted to compute the binding free energies (i.e., potential of mean force (PMF)) of CH_3CH_3 , CH_3CONH_2 and CH_3OH to ice prism surface, respectively. We first build the ice slab system, which contains one layer of ice molecules (60 molecules) with dimensions $2.27 \text{ nm} \times 2.22 \text{ nm} \times 10.0 \text{ nm}$. Then, about 900 water molecules and 1 solute molecule are added to the systems. The temperature is set to 280 K to avoid freezing. The initial ice molecules are harmonically restrained at their original positions with a force constant of $3000 \text{ kJ mol}^{-1} \text{ nm}^{-2}$ to avoid the melting of ice surface. The center of mass distance along the Z-axis between the gas molecule and ice surface is considered as the reaction coordinate (RC) and the Z distance along the RC (~2.0 nm) is divided into windows every 0.02 nm. A harmonic umbrella potential with a force constant of $1000 \text{ kJ mol}^{-1} \text{ nm}^{-2}$ is applied along the Z-axis. In each umbrella window, a 500 ps equilibration simulation followed by a 20 ns production run is performed under the NVT ensemble. The PMFs are constructed by the weighted histogram analysis method [77] and plotted as a function of the distance from ice surface. We set the average PMF at distances from 1.4 to 1.8 nm as the reference point since the water molecules in this region can be considered as bulk water.

2.4. Adsorption Energies

The adsorption energies of CH_3CH_3 , CH_3CONH_2 and CH_3OH on ice prism surface are calculated using the Vienna Ab-initio Simulation Package (VASP) code [78,79], where the core electrons are treated with the projector augmented-wave (PAW) method [80,81]. The valence electrons for all systems are described using the generalized gradient approximation (GGA) with the Perdew–Burke–Ernzerhof (PBE) function [82]. The DFT-D3 correction method of Grimme et al. [83]. is employed to describe the van der Waals interactions. The Brillouin-zone sampling is restricted to the Γ -point [84] because of the large supercell size used in the calculations. The energy cutoff for the plane wave basis sets is set to 600 eV and the electron smearing is described by the Gaussian smearing method [85] with a width of 0.05 eV. Each calculation is considered converged when the total energy changed is less than 10^{-5} eV and the forces on each atom are smaller than 0.05 eV/Å. The whole simulation box is set to $18.2 \times 14.8 \times 23.1 \text{ \AA}^3$ containing a vacuum of ~18 Å and two layers

of 2×2 ice Ih. The top layer of the ice is allowed to move freely, and the bottom layer of the ice is fixed to describe the bulk ice. Several representative adsorption sites are calculated and we present the most stable one. The adsorption energies of CH_3CH_3 , CH_3CONH_2 and CH_3OH molecules on the ice prism surface are calculated as

$$E_{ads} = (E_A + E_B) - E_{AB} \quad (1)$$

where E_A and E_B are the total energy of molecules in the gas phase and the relaxed ice prism surface system, respectively. E_{AB} is the energy of the adsorption system. Larger adsorption energy represents a more stable adsorption.

2.5. Water Dynamics and Flexibility Analyses

In order to compare the dynamics and flexibility of each part of AFGP8 in solution, an AFGP8 is put into a cubic box and then solvated by ~2900 water molecules. Each system is firstly subjected to a steepest-descent energy minimization with a tolerance of $1000 \text{ kJ mol}^{-1} \text{ nm}^{-1}$, followed by a 500 ps equilibration NPT-MD simulation at 268 and 300 K. Finally, 60 ns production NPT-MD run is evolved at 268 and 300 K. The intermittent hydrogen bond autocorrelation function [86,87] is calculated as

$$C_{HB}(t) = \frac{\langle h(0)h(t) \rangle}{\langle h(0)h(0) \rangle} \quad (2)$$

where the value of $h(t)$ equals 1 if a tagged pair of different molecules are hydrogen bonded at the time origin and still exists at time t and 0 if the hydrogen bond is absent. The average is taken over different time origins and all possible pairs.

To represent the relative mobility of different groups and the flexibility of AFGP8, we calculate the mean-squared displacement (MSD) and the B factors [88]. The former is calculated as

$$MSD = \langle |\vec{r}_i(t) - \vec{r}_i(0)|^2 \rangle_{i \in A} \quad (3)$$

where the average is taken over different time origins and all particles of type A. The B factor is gained as follows

$$RMSF_i = \sqrt{\frac{\sum_{t_0}^t [r_i(t') - \bar{r}_i]^2}{t - t_0}} \quad (4)$$

$$RMSF = \frac{\sum_i RMSF_i \cdot m_i}{\sum_i m_i} \quad (5)$$

$$B = RMSF^2 \cdot \frac{8}{3} \pi^2 \quad (6)$$

where r_i and m_i represent the position and the mass of atom i in conceded residue, respectively.

3. Results and Discussion

3.1. PPII Helix Conformations Are the Dominant Structures of AFGP8

To rationalize the conformations of AFGP8 in solution, we performed REMD simulations. Figure 1c shows the distribution of the radius of gyration (R_g) for AFGP8 at 268 and 300 K. Consistent with a previous nuclear magnetic resonance (NMR) spectroscopy study [89], it shows an obvious pick at 1.1–1.2 nm for both temperatures, suggesting that the structure of AFGP8 is adequately extended in solution. Further statistics of dihedral angles between amino acids (the Ramachandran plots) of AFGP8 shown in Figure 1d,e depict that the PPII helix is the dominant conformation of AFGP8 in solution for both temperatures, which is consistent with previous reports [42,45,47,90,91] and corresponds to the peak of the distribution of R_g . In addition, the PPII helix becomes more pronounced at a lower temperature, indicating that AFGP8 mainly adopts the extended conformation with high population of the PPII helix at subzero temperature (268 K).

3.2. Both Hydrogen-Bonding and Hydrophobic Groups Synergistically Contribute to the IRI Activity of AFGP8

In the MD modeling of antifreeze material, such as PVA and AF(G)Ps, the initial structure has a vital influence on its IRI activity [45,56]. Aiming to systematically investigate its IRI activity, we set up a series of MD simulations at 268 K of AFGP8 with the PPII helix, in which different groups are contacting with ice prism surface. All the simulations are performed for at least 1000 ns to monitor the IRI activity. The dependence of IRI activities on the binding strength of AFGP8 to ice is represented in Figure 2. In about 70% of our simulations, we observe that AFGP8 obviously slows down the growth rate of ice compared to the case of pure water but is still pushed along with the growing ice front (Figure 3a), which is denoted as weak binding (WB). In this case, AFGP8 “walks” irregularly on ice surfaces leading to the reversible binding of AFGP8 to ice (Figure 3b). However, we find that for about 20% of our simulations AFGP8 can bind to ice irreversibly through the backbone, which lies flat on the ice surface with most of the methyl ($-\text{CH}_3$) and amide ($-\text{CONH}-$, on the backbone) groups being adsorbed to the ice surface and dramatically prevents the growth of the ice front, as shown in Figure 3c,d. In this case, the $-\text{CH}_3$ groups occur at the cavities of ice through hydrophobic effect and the $-\text{CONH}-$ groups anchor to the ice surface by forming hydrogen bonds with ice directly. The disaccharides float in the water phase with almost no hydrogen bond being formed between disaccharides and ice. As a result, we ascribe this irreversible binding to the synergistic effect of the hydrophobic interaction of $-\text{CH}_3$ groups and hydrogen bonding between $-\text{CONH}-$ groups and ice and refer to this case as backbone dominant binding (BDB), which has not been reported before. Additionally, we find another case of irreversible binding in our simulations (10%), where the disaccharide of AFGP8 inserts into the ice steps and some $-\text{CH}_3$ groups on the backbone are also adsorbed to the ice front, see Figure 3e,f. In this case, the $-\text{OH}$ group on the disaccharides instead of the $-\text{CONH}-$ group on the backbone anchors to the ice surface by forming hydrogen bonds with ice directly, which is denoted as disaccharide dominant binding (DDB). Furthermore, it is discovered that the binding strengths of AFGP8 to ice are comparable for both DDB and BDB.

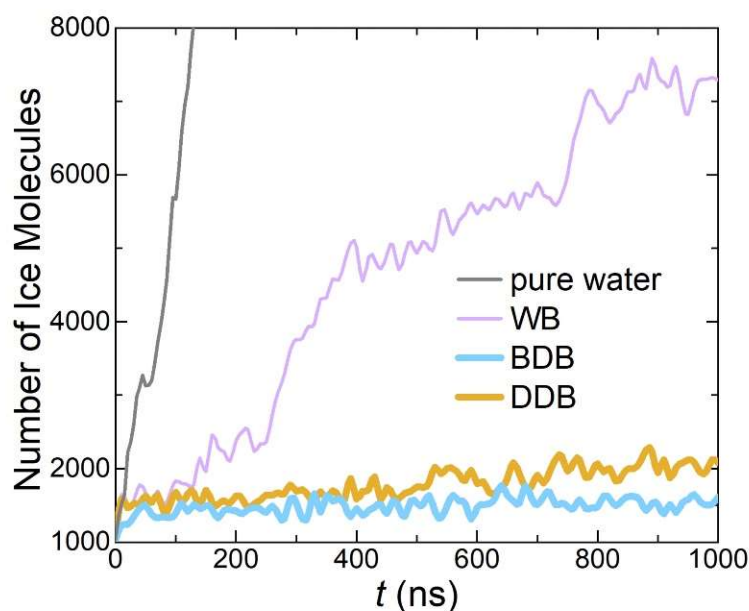


Figure 2. AFGP8 inhibits ice growth. The growth of ice on prism surface at 268 K in pure water (gray line) and AFGP8 solutions. Three binding cases of AFGP8: weak binding (purple line), backbone dominant binding (cyan line) and disaccharide dominant binding (orange line).

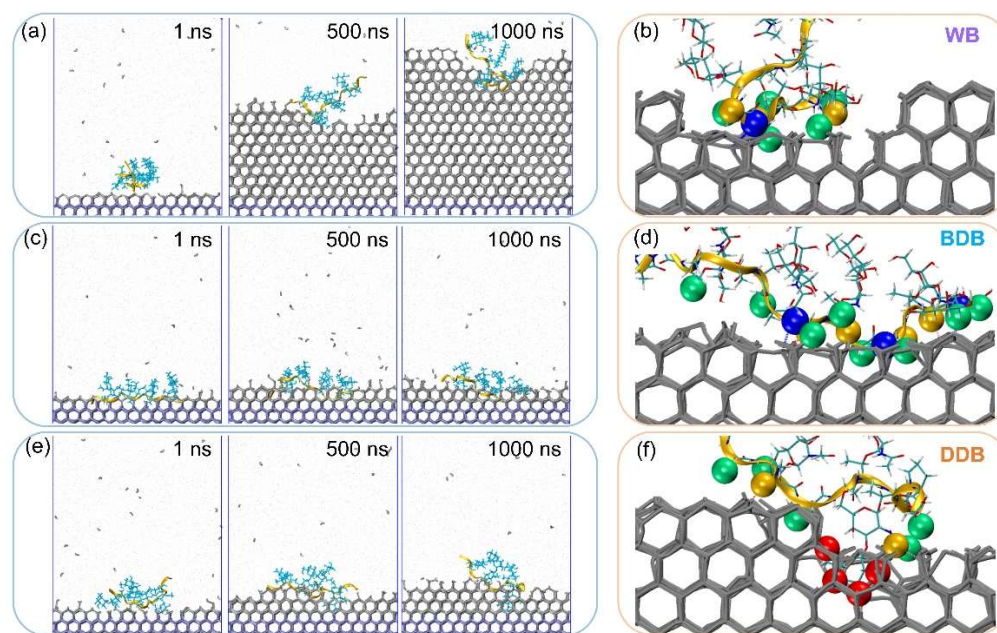


Figure 3. Hydrogen-bonding and hydrophobic groups contribute to the binding of AFGP8 to ice. Different representative snapshots (1 ns, 500 ns, 1000 ns, respectively) of three binding cases: weak binding (a), backbone dominant binding (c) and disaccharide dominant binding (e). The detailed binding cases are enlarged in panel (b,d,f), respectively. The bottom two layers of ice, colored in ice blue, are restrained by a harmonic potential. The free ice and liquid water molecules are shown by gray lines and gray dots, respectively. The color coding: methyl groups (green balls), O (orange balls) and N (blue balls) of amide groups and hydroxyl groups (red balls); the backbone of AFGP8 (orange ribbon), Thr residues (cyan or colorful licorice).

In order to quantitatively investigate the cases of WB, BDB and DDB, we elucidate the concrete roles of the $-\text{CH}_3$, $-\text{CONH}-$ and $-\text{OH}$ groups of AFGP8 played in the IRI activity of the three cases by analyzing the average number of $-\text{CH}_3$ groups (N_{CH_3}) interacting with ice and the hydrogen bonds formed by the $-\text{CONH}-$ (N_{CONH}) or $-\text{OH}$ (N_{OH}) groups with ice, as shown in Figure 4. We find that AFGP8 binds to ice through the co-adsorption of the hydrogen-bonding and hydrophobic groups in all three cases. For the case of WB, we note that N_{CH_3} , N_{CONH} and N_{OH} are only limitedly verifiable (~ 4 , ~ 2 and ~ 2 , respectively). This might be the main reason for their reversible binding. In contrast to WB, N_{CH_3} (~ 12) and N_{CONH} (~ 8) are significantly increased, but N_{OH} is even lower (~ 1) in BDB, which suggests that the $-\text{CH}_3$ and $-\text{CONH}-$ groups play a key role in the irreversible binding of AFGP8 to ice. For the case of DDB, N_{CH_3} is similar with WB but its IRI activity is greatly improved compared to WB. This can be attributed to the significant increasing of N_{OH} (~ 6), which demonstrates that the $-\text{OH}$ group can also play as key for the binding of AFGP8 to ice. Our results directly provide theoretical evidence for previous experiments [50] where $-\text{OH}$ groups are indispensable for the significant antifreeze activity of AFGP8.

However, the contributions of the $-\text{CH}_3$ and $-\text{CONH}-$ groups to the IRI activity are difficult to distinguish because they are almost adjacent to each other in AFGP8 (Figure 1a,b). To demonstrate the role of the $-\text{CONH}-$ groups in IRI activity, we design a model molecule of GLY14 ($[\text{Gly-Gly-Gly}]_4\text{-Gly-Gly}$) that consists of $-\text{CONH}-$ groups only and perform MD simulations to investigate its IRI activity, see Figure 5. We find that the ice growth inhibition mechanism of fully flexible GLY14 is similar to that of PVA, where the binding mainly occurs from hydrogen bonding and its contact area with ice surface dictates the IRI activity [56]. GLY14 binds to ice sufficiently well and effectively inhibits the growth of ice until it is overgrown or pushed away (~ 250 ns in Figure 5b) by the advancing ice front of the ice prism surface. This is because the contact area of GLY14 with the ice surface decreases as it is deformed by the growth of the ice front due to its great hydrophilicity and

full flexibility. On the other hand, experimental studies have shown that the amphiphilicity is necessary for high IRI activity of AFGPs, and excessive hydrophilicity or hydrophobicity is not conducive to its antifreeze activity [37,46,50,60,67]. Therefore, we speculate that a strong IRI activity needs a synergy of sufficient hydrogen-bonding ($-\text{OH}$ or $-\text{CONH}-$) and hydrophobic ($-\text{CH}_3$) groups in AFGP8 to bind to ice.

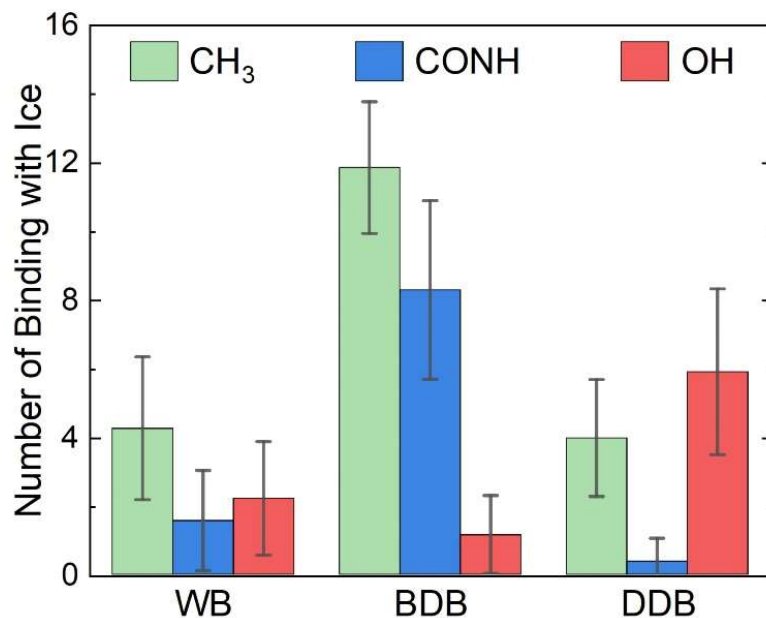


Figure 4. The $-\text{CH}_3$, $-\text{CONH}-$ and $-\text{OH}$ groups play a crucial role in the binding of AFGP8 to ice. The average number of methyl groups (green rectangles) interact with ice and the average hydrogen bonds of amide groups (blue rectangles) or hydroxyl groups (red rectangles) interact with ice, in the cases of weak binding (WB), backbone dominant binding (BDB) and disaccharide dominant binding (DDB), respectively.

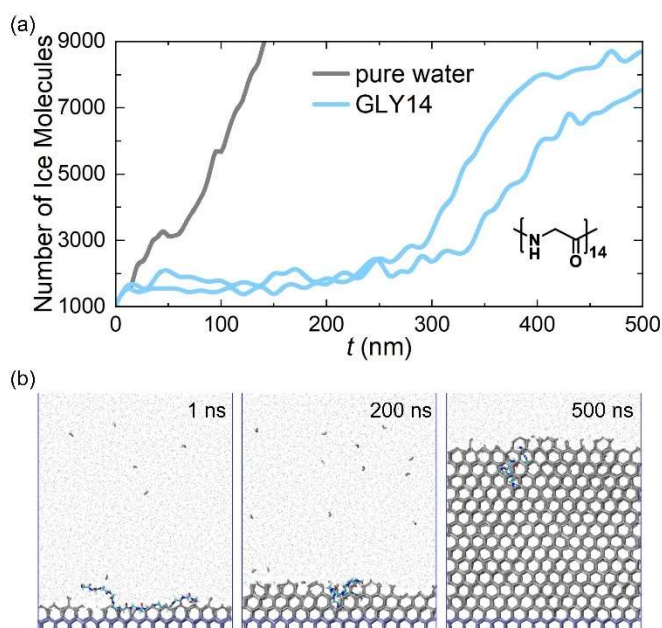


Figure 5. GLY14 can also bind to ice surfaces. (a) The structure and ice growth inhibition performance of GLY14. (b) Representative snapshots of simulations (1 ns, 200 ns and 500 ns, respectively). The free ice and liquid water molecules are shown by gray lines and gray dots, respectively. The GLY14 is represented as colorful licorice.

3.3. Hydrophobic Desolvation and Hydrogen Bonding Drive the Binding of AFGP8 to Ice

We have shown that the $-\text{CH}_3$, $-\text{CONH}-$ and $-\text{OH}$ groups of AFGP8 contribute to its IRI activity. In order to clarify the driving force behind the binding of AFGP8 to ice, we seek to perform enthalpic and entropic analyses in terms of adsorption energy and free energy calculations. We saturate the three groups with methyl to obtain CH_3CH_3 , CH_3CONH_2 and CH_3OH molecules and calculate the adsorption energy of the three molecules on the ice Ih prism surface. By taking the adsorption energy of water molecules (~ 0.51 eV in Figure 6a) as a reference, we show that the adsorption energy of CH_3CONH_2 (~ 0.85 eV), which forms double hydrogen bonds to the ice surface, is much larger than water molecule adsorption, indicating the less electronegative nature of the nitrogen atom with respect to the oxygen atom. CH_3OH exhibits a similar adsorption energy of ~ 0.45 eV as water molecules because CH_3OH also adsorbs to the ice surface by forming an O–H–O hydrogen bond. For CH_3CH_3 , no hydrogen is formed and the so-called “adsorption energy” of CH_3CH_3 is small (~ 0.19 eV). We interpret that the $-\text{CH}_3$ group is passively deposited on the ice surface under hydrophobic desolvation. The free energy calculation (Figure 6b) further confirms our explanation of $-\text{CH}_3$ deposited on the ice surface. With the inclusion of the water phase, the free energy of CH_3CH_3 exhibits two minima, corresponding to the molecule in contact with ice and the ice-like water layer. Similarly, the free energies of CH_3CONH_2 and CH_3OH also show two minima near the ice surface, suggesting that all three groups prefer to stay in the region of the ice/water interface. We note that the second minimum of the free energy of CH_3CH_3 is smaller than the first but CH_3OH shows a deeper first minimum. This suggests that the $-\text{OH}$ group provides a stronger direct adsorption on the ice surface with respect to the $-\text{CH}_3$ group and prevents AFGP8 from being pushed away by the growing ice front. That is why, in the case of DDB, the AFGP8 hinders ice growth with only one disaccharide anchoring to ice. Additionally, despite the free energy of CH_3CONH_2 being equally conducive for $-\text{CONH}-$ to stay on ice surface or ice-like water layer, the enthalpic contribution (adsorption energy) may be stable $-\text{CONH}-$ groups on the ice surface by hydrogen bonding. This suggests that when there are enough $-\text{CONH}-$ and $-\text{CH}_3$ groups being adsorbed to the ice surface, AFGP8 can also bind to ice tightly (i.e., in the case of BDB). To conclude, the binding affinity to the ice surface is relevant to the contribution of both enthalpy and entropy, associated with the formation of hydrogen bonds and the desolvation of the $-\text{CH}_3$ groups, respectively. Moreover, the hydrophobic desolvation and hydrogen bonding synergistically promote the binding of AFGP8 to ice.

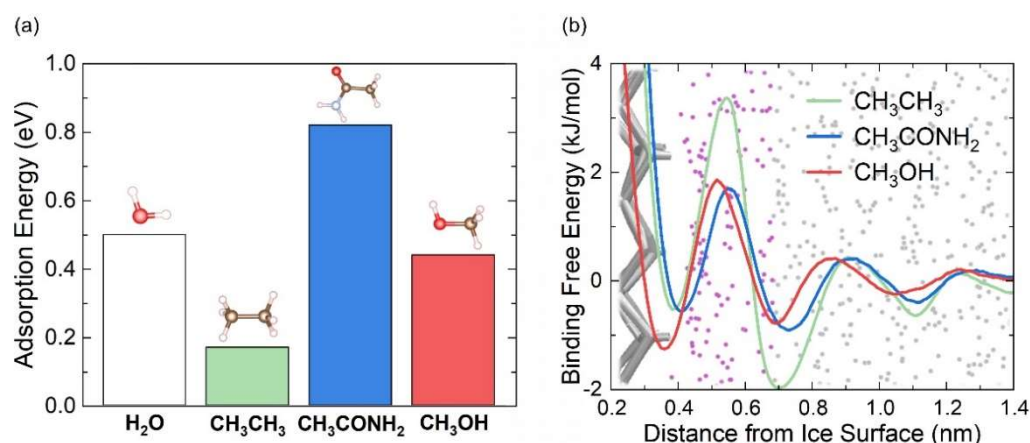


Figure 6. Hydrogen bonding and hydrophobic desolvation are the driving forces for the binding of AFGP8 to ice. (a) Adsorption energies of water (colorless rectangle), ethane (green rectangle), acetamide (blue rectangle) and methyl alcohol (red rectangle) on the prism surface of ice Ih. (b) Binding free energy of ethane (green line), acetamide (blue line) and methyl alcohol (red line) to the prism surface. The background: ice (silver stick), ice-like layer (purple dot) and liquid water (silver dot).

It is also observed that the $-\text{CH}_3$ groups are mainly adsorbed to the S and W sites (Figure 7a) on the ice surface, in agreement with previous work [45]. Instead, the $-\text{CONH}-$ and $-\text{OH}$ groups tend to be adsorbed at the Hex site (as shown in Figure 7a, the H or O of the surface ice molecule) through hydrogen bonding. Moreover, we note that N and O atoms in the $-\text{CONH}-$ group can form hydrogen bonds with ice at the Hex sites. This indicates that the $-\text{CONH}-$ group has more ice-binding sites than the $-\text{OH}$ group, which may be one of the reasons why the case of BDB is easier to be observed than DDB in simulation. In addition, the “distance matching” between certain groups in antifreeze agents and water molecules at the ice surface is also critical for the binding of antifreeze agents to ice [57,58,92–94]. The nearest neighbor distance between the $-\text{CH}_3$ group and the O/N atom in $-\text{CONH}-$ is about 4.0/4.5 Å. Moreover, the distance between the S/W and Hex sites of ice is about 5.0 Å and 5.3 Å (Figure 7a), respectively. The proper distances between the $-\text{CH}_3$ groups and $-\text{CONH}-$ groups can have a significant “stereoscopic match” with the binding site on ice surfaces due to the flexibility of hydrogen bonds, and the $-\text{CH}_3$ group can be further stabilized on ice surfaces by its adjacent $-\text{CONH}-$ group, which binds to ice through directly hydrogen bonding. Thus, they can cooperatively promote the binding of AFGP8 to ice (Figure 7b). This might be one of the reasons why the IRI activity of AFGP8 is orders of magnitude better than PVAs. From the above analysis, we argue that hydrogen-bonding and hydrophobic groups contribute equally to the binding of AFGP8 to ice, in which the hydrophobic groups help AFGP8 to make contact with ice surfaces and the hydrogen-bonding groups anchor AFGP8 on ice surfaces.

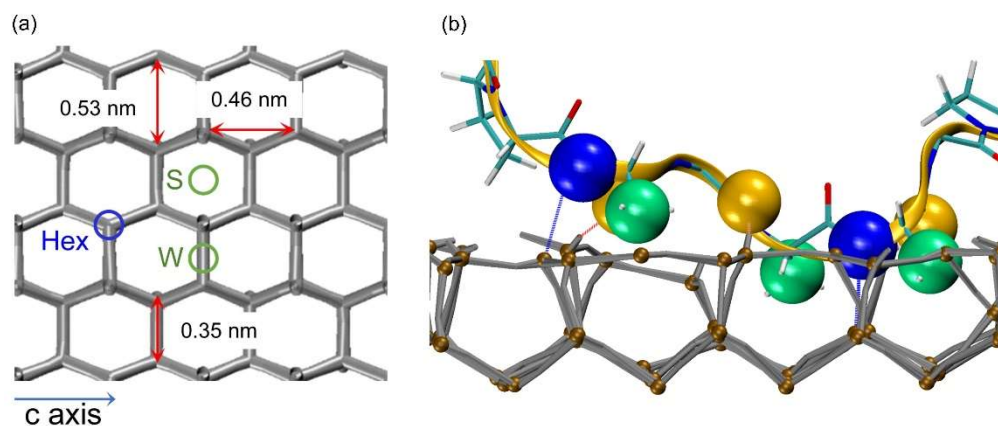


Figure 7. Amide groups and methyl groups cooperatively promote the binding of AFGP8 to ice. (a) The lattice parameters of ice Ih prism surface (red double arrow line) and the binding sites of AFGP8 on ice prism surface. S and W (green circles) are the binding sites of methyl groups. Hex (blue circles) are the binding sites of amide groups (including hydroxy groups), representing the top of O or H atoms at the vertex of the ice hexagon. (b) Co-adsorption of methyl groups and amide groups on ice prism surfaces. The color coding: methyl groups (green balls), O (orange balls) and N (blue balls) of amide groups; the backbone of AFGP8 (orange ribbon and colorful sticks); hydrogen bonds (red or blue dashed lines).

3.4. AFGP8 Perturbs the Water Dynamics

Previous works have suggested that AFGPs can also inhibit the growth of ice by perturbing water dynamics [46,95–97]. To explore the influence of different groups in AFGP8 on water dynamics, we further analyze the structural relaxation of hydrogen bonds via the intermittent hydrogen bond autocorrelation function $C_{\text{HB}}(t)$, as shown in Figure 8. Obviously, the $C_{\text{HB}}(t)$ between $-\text{CONH}-$ groups and water decays more slowly than that between $-\text{OH}$ groups and water (Figure 8a), which hints that the $-\text{CONH}-$ group of AFGP8 has more stable hydrogen bonding with adjacent water molecules. In this regard, we conjecture that the $-\text{CONH}-$ groups of AFGP8 may be more steadily adsorbed on ice surfaces than $-\text{OH}$ groups. We also note that the $C_{\text{HB}}(t)$ between hydrogen-bonding ($-\text{CONH}-$ or $-\text{OH}$) groups and water decays significantly slower than that of

water (Figure 8a,b), suggesting that $-\text{CONH}-$ and $-\text{OH}$ groups that stay in the ice-like water layer can capture the surrounding water molecules and block the diffusion of water onto the ice surface, thus further reducing the growth rate of ice. Overall, AFGP8 slows down the dynamics of the surrounding water and perturbs the hydrogen bond network of ice-like water (insert of Figure 8b), which is consistent with previous experimental reports [33,95] and simulation studies [46,96,98]. Therefore, it is evident that AFGP8 inhibits ice growth not only by direct adsorption but also by slowing down the dynamics of the surrounding water.

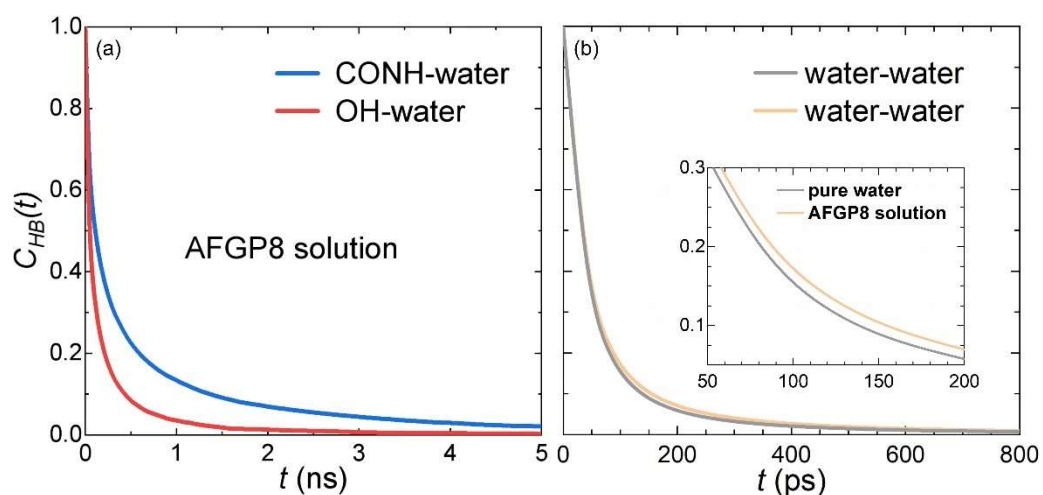


Figure 8. AFGP8 perturbs the hydrogen bond network of water. (a) The intermittent hydrogen bond autocorrelation functions of amide-water (blue line) and hydroxyl-water (red line) of AFGP8 in water at 268 K. (b) The water–water intermittent hydrogen bond autocorrelation functions in pure-water (black line) and AFGP8 solution (orange line) at 268 K.

3.5. The Flexible Disaccharides Are as Useful as the Rigid Backbone in Anti-Freezing

In our simulations, we observe that AFGP8 can automatically explore the appropriate binding position on the ice surface. Although it has been explained by the great flexibility of AFGP8 [45], the specific contribution of different residues of AFGP8 to its flexibility is still elusive. Here, we analyze the mobility of different groups of AFGP8 in solution by computing the mean squared displacement (*MSD*), as shown in Figure 9a. The result indicates that the sequence of the mobility of these three groups is: $-\text{OH} > -\text{CH}_3 > -\text{CONH}-$, whether at 268 or 300 K. This may explain why the $C_{\text{HB}}(t)$ between $-\text{CONH}-$ groups and water decays more slowly than that between $-\text{OH}$ and water. To further visualize the flexibility of each residue of AFGP8, we calculate the B factor of AFGP8, see Figure 9b. Clearly, the disaccharide of AFGP8 is more flexible than the peptide. This suggests that the backbone is harder to break off once it binds to the ice surfaces due to its slight rigidity; thereby, it may bind to ice more easily than the disaccharides. Accordingly, the disaccharides are slightly harder to anchor to the ice surface firmly, which requires forming multiple hydrogen bonds with ice simultaneously. This may explain why most of the disaccharide chains of AFGP8 stay in solution and the case of BDB is more common than DDB in simulations. On the other hand, these disaccharides in solution can slow down the dynamics of the surrounding water and prevent water molecules from entering the ice surfaces, thus further enhancing the IRI activity of AFGP8. Combining the idea that high affinity to water is necessary for the effective separation of some IRI agents in the ice-water interface and gaining a high IRI activity proposed by Wang et al. [99], the more flexible and hydrophilic disaccharides may facilitate AFGP8 diffusion through the ice surfaces until finding the suitable adsorption sites and cover a wider area of ice surfaces to gain a better antifreeze activity. Therefore, we argue that both the highly flexible disaccharide motifs and the appropriately rigid backbone play a crucial role in the individual antifreeze effect of AFGP8.

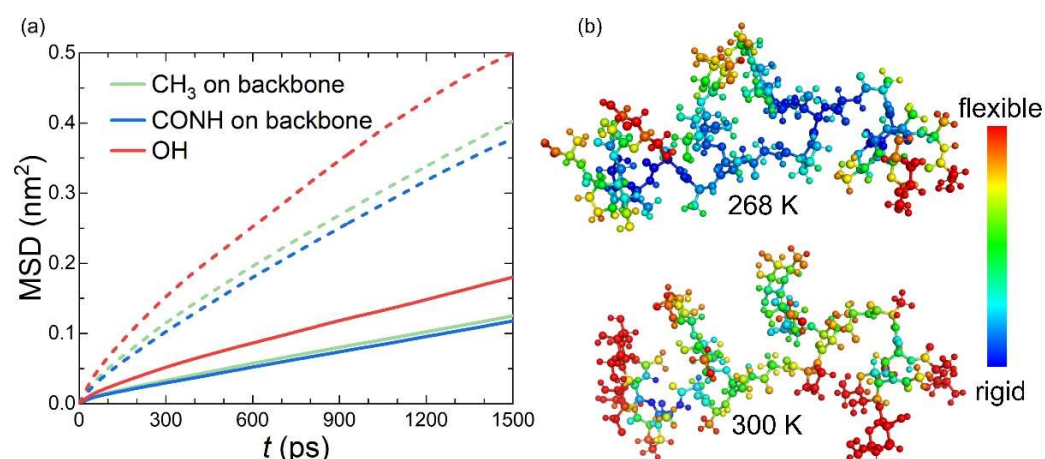


Figure 9. The disaccharides of AFGP8 are more flexible than its backbone. (a) Mean squared displacement of methyl groups on backbone (green lines), amide groups (blue lines) and hydroxyl groups (red lines) at 268 K (solid lines) and 300 K (dashed lines). (b) Flexibility (B factors) of AFGP8 at 268 and 300 K.

4. Conclusions

We combine all-atom molecular dynamics simulations and density functional theory (DFT) calculations to systematically elucidate the ice growth inhibition mechanism of AFGP8 and the roles of $-\text{CH}_3$, $-\text{CONH}-$ and $-\text{OH}$ groups in the binding of AFGP8 to ice. On the one hand, AFGP8 can inhibit ice growth by an adsorption mechanism. Our simulations indicate that both the backbone and disaccharides can bind to ice, and the binding of AFGP8 to ice is driven by the synergistic effect of hydrophobic desolvation and hydrogen bonding. The bindings can be divided into three cases: WB, BDB and DDB. The reversible (WB) and irreversible (BDB and DDB) binding between protein and ice surfaces are obviously observed on our finite simulation time scale (1000 ns) and the supercooling condition (268 K), and the binding strengths of AFGP8 to ice are comparable for both DDB and BDB. On the other hand, AFGP8 also enhances IRI activity by slowing down the dynamics of the surrounding water and perturbing the hydrogen bond network. The disaccharides are generally more flexible than the backbone and most of them prefer to sway in solution and perturb the water dynamics, therefore further enhancing the IRI activity of AFGP8.

Furthermore, our results show that the hydrophobic ($-\text{CH}_3$) and hydrogen-bonding ($-\text{CONH}-$ or $-\text{OH}$) groups contribute equally to the binding of AFGP8 to ice, and synergistically promote this binding. Specifically, the $-\text{CH}_3$ groups promote AFGP8 contact with ice surfaces through hydrophobic interaction, while the $-\text{CONH}-$ and $-\text{OH}$ groups anchor the backbone and disaccharides to ice surfaces through direct hydrogen bonding, respectively. The binding affinity of these three groups is relevant to not only the subtle contribution of both enthalpic and entropic interactions but also the local topology of the complicated protein or ice surface. In particular, the ancillary simulations of GLY14 indicate that the $-\text{CONH}-$ group also plays an important role in the IRI activity. Additionally, the $-\text{OH}$ groups on the disaccharides of AFGP8 more easily perturb the water dynamic due to their high mobility and strong hydrogen bonding. It is also observed in our simulation that the $-\text{CONH}-$ groups on the disaccharide moieties can directly bind to ice, which is consistent with the experiment result that the N-acetyl groups are important for the extraordinary antifreeze activity of AFGP8 [60]. Based on our results, we suggest the following for the design of highly effective flexible IRI agents: (1) A separation of the relatively hydrophobic rigid backbone and hydrophilic flexible side chains is necessary, the rigid part is easier to bind to ice and the flexible side chains can bind to ice and perturb the dynamics of the surrounding water; (2) Enough ice binding sites (hydrogen-bonding and hydrophobic groups) are required; thereby, the IRI agents can bind to ice strongly with a variety of configurations

and gain a high IRI activity; (3) The hydrogen-bonding groups and hydrophobic groups need to be spatially distributed in a way that fits the ice structure, promoting the binding of IRI agents to ice through synergistic effects. Overall, this work enhances the understanding of the IRI mechanisms of AFGPs at the molecular level and has important implications for guiding the design of more refined materials with high antifreeze activity for medical and industrial, as well as agricultural applications.

Author Contributions: W.Y., Q.S. and Z.S. designed research; W.Y. performed research; W.Y., Y.L., Q.S. and Z.S. contributed the analytic methods; W.Y., Q.S. and Z.S. analyzed data; and W.Y. and Z.S. wrote the paper. All authors have read and agreed to the published version of the manuscript.

Funding: This research was funded by the National Natural Science Foundation of China (Grant No. 12104306).

Data Availability Statement: The data presented in this study are available on request.

Acknowledgments: The authors gratefully acknowledge the financial support from the National Natural Science Foundation of China (12104306) and Shanghai Tech start-up funding. The computational resources are provided by ShanghaiTech University.

Conflicts of Interest: There are no conflict of interest to declare.

References

1. Feeney, R.; Burcham, T.; Yeh, Y. Antifreeze glycoproteins from polar fish blood. *Ann. Rev. Biophys. Biophys. Chem.* **1986**, *15*, 59–78. [[CrossRef](#)]
2. Duman, J.G. Antifreeze and Ice Nucleator Proteins in Terrestrial Arthropods. *Annu. Rev. Physiol.* **2001**, *63*, 327–357. [[CrossRef](#)]
3. DeVries, A.L.; Wohlschlag, D.E. Freezing resistance in some Antarctic fishes. *Science* **1969**, *163*, 1073–1075. [[CrossRef](#)]
4. DeVries, A.L. Glycoproteins as Biological Antifreeze Agents in Antarctic Fishes. *Science* **1971**, *172*, 1152–1155. [[CrossRef](#)]
5. Bar Dolev, M.; Braslavsky, I.; Davies, P.L. Ice-Binding Proteins and Their Function. *Annu. Rev. Biochem.* **2016**, *85*, 515–542. [[CrossRef](#)]
6. Carpenter, J.F.; Hansen, T.N. Antifreeze protein modulates cell survival during cryopreservation: Mediation through influence on ice crystal growth. *PNAS* **1992**, *89*, 8953–8957. [[CrossRef](#)]
7. Liu, X.; Pan, Y.; Liu, F.; He, Y.; Zhu, Q.; Liu, Z.; Zhan, X.; Tan, S. A Review of the Material Characteristics, Antifreeze Mechanisms, and Applications of Cryoprotectants (CPAs). *J. Nanomater.* **2021**, *2021*, 9990709. [[CrossRef](#)]
8. Yang, J.; Liu, M.; Zhang, T.; Ma, J.; Ma, Y.; Tian, S.; Li, R.; Han, Y.; Zhang, L. Cell-friendly regulation of ice crystals by antifreeze organism-inspired materials. *AIChE J.* **2022**, *68*, e17822. [[CrossRef](#)]
9. Biggs, C.I.; Bailey, T.L.; Ben, G.; Stubbs, C.; Fayter, A.; Gibson, M.I. Polymer mimics of biomacromolecular antifreezes. *Nat. Commun.* **2017**, *8*, 1546. [[CrossRef](#)]
10. Kim, H.J.; Lee, J.H.; Hur, Y.B.; Lee, C.W.; Park, S.-H.; Koo, B.-W. Marine Antifreeze Proteins: Structure, Function, and Application to Cryopreservation as a Potential Cryoprotectant. *Mar. Drugs.* **2017**, *15*, 27. [[CrossRef](#)]
11. Liu, Z.; Zheng, X.; Wang, J. Bioinspired Ice-Binding Materials for Tissue and Organ Cryopreservation. *J. Am. Chem. Soc.* **2022**, *144*, 5685–5701. [[CrossRef](#)]
12. Tian, J.; Walayat, N.; Ding, Y.T.; Liu, J.H. The role of trifunctional cryoprotectants in the frozen storage of aquatic foods: Recent developments and future recommendations. *Compr. Rev. Food Sci. Food Saf.* **2022**, *21*, 321–339. [[CrossRef](#)]
13. Hassas-Roudsari, M.; Goff, H.D. Ice structuring proteins from plants: Mechanism of action and food application. *Food Res. Int.* **2012**, *46*, 425–436. [[CrossRef](#)]
14. Zhu, S.C.; Yu, J.H.; Chen, X.; Zhang, Q.; Cai, X.X.; Ding, Y.T.; Zhou, X.X.; Wang, S.Y. Dual cryoprotective strategies for ice-binding and stabilizing of frozen seafood: A review. *Trends Food Sci. Technol.* **2021**, *111*, 223–232. [[CrossRef](#)]
15. Andersson, A.K.; Chapman, L. The impact of climate change on winter road maintenance and traffic accidents in West Midlands, UK. *Accid. Anal. Prev.* **2011**, *43*, 284–289. [[CrossRef](#)]
16. Lv, J.; Song, Y.; Jiang, L.; Wang, J. Bio-Inspired Strategies for Anti-Icing. *ACS Nano* **2014**, *8*, 3152–3169. [[CrossRef](#)]
17. Li, Q.; Guo, Z. Fundamentals of icing and common strategies for designing biomimetic anti-icing surfaces. *J. Mater. Chem. A* **2018**, *6*, 13549–13581. [[CrossRef](#)]
18. Meng, Y.; Zhao, Q.; Lei, J.; Mao, M.; Qin, Y.; Xi, C.; Lu, Z.; Yang, X.; Rong, H. Preparation of biological antifreeze protein-modified emulsified asphalt coating and research on its anti-icing performance. *Constr. Build. Mater.* **2021**, *294*, 123473. [[CrossRef](#)]
19. Raymond, J.A.; Fritsen, C.H. Semipurification and Ice Recrystallization Inhibition Activity of Ice-Active Substances Associated with Antarctic Photosynthetic Organisms. *Cryobiology* **2001**, *43*, 63–70. [[CrossRef](#)]
20. Knight, C.A.; Duman, J.G. Inhibition of recrystallization of ice by insect thermal hysteresis proteins: A possible cryoprotective role. *Cryobiology* **1986**, *23*, 256–262. [[CrossRef](#)]

21. Kristiansen, E.; Zachariassen, K.E. The mechanism by which fish antifreeze proteins cause thermal hysteresis. *Cryobiology* **2005**, *51*, 262–280. [[CrossRef](#)]
22. Oude Vrielink, A.S.; Aloï, A.; Olijve, L.L.; Voets, I.K. Interaction of ice binding proteins with ice, water and ions. *Biointerphases* **2016**, *11*, 018906. [[CrossRef](#)]
23. Ghalamara, S.; Silva, S.; Brazinha, C.; Pintado, M. Structural diversity of marine anti-freezing proteins, properties and potential applications: A review. *Bioresour. Bioprocess.* **2022**, *9*, 5. [[CrossRef](#)]
24. Scotter, A.J.; Marshall, C.B.; Graham, L.A.; Gilbert, J.A.; Garnham, C.P.; Davies, P.L. The basis for hyperactivity of antifreeze proteins. *Cryobiology* **2006**, *53*, 229–239. [[CrossRef](#)] [[PubMed](#)]
25. Briard, J.G.; Poisson, J.S.; Turner, T.R.; Capicciotti, C.J.; Acker, J.P.; Ben, R.N. Small molecule ice recrystallization inhibitors mitigate red blood cell lysis during freezing, transient warming and thawing. *Sci. Rep.* **2016**, *6*, 23619. [[CrossRef](#)] [[PubMed](#)]
26. Graham, B.; Fayter, A.E.R.; Houston, J.E.; Evans, R.C.; Gibson, M.I. Facially Amphipathic Glycopolymers Inhibit Ice Recrystallization. *J. Am. Chem. Soc.* **2018**, *140*, 5682–5685. [[CrossRef](#)] [[PubMed](#)]
27. Tam, R.Y.; Ferreira, S.S.; Czechura, P.; Chaytor, J.L.; Ben, R.N. Hydration Index—A Better Parameter for Explaining Small Molecule Hydration in Inhibition of Ice Recrystallization. *J. Am. Chem. Soc.* **2008**, *130*, 17494–17501. [[CrossRef](#)]
28. Balcerzak, A.K.; Capicciotti, C.J.; Briard, J.G.; Ben, R.N. Designing ice recrystallization inhibitors: From antifreeze (glyco)proteins to small molecules. *RSC Adv.* **2014**, *4*, 42682–42696. [[CrossRef](#)]
29. Mitchell, D.E.; Fayter, A.E.; Deller, R.C.; Hasan, M.; Gutierrez-Marcos, J.; Gibson, M.I. Ice-recrystallization inhibiting polymers protect proteins against freeze-stress and enable glycerol-free cryostorage. *Mater. Horiz.* **2019**, *6*, 364–368. [[CrossRef](#)]
30. Gibson, M.I.; Barker, C.A.; Spain, S.G.; Albertin, L.; Cameron, N.R. Inhibition of Ice Crystal Growth by Synthetic Glycopolymers: Implications for the Rational Design of Antifreeze Glycoprotein Mimics. *Biomacromolecules* **2009**, *10*, 328–333. [[CrossRef](#)]
31. Warren, M.T.; Galpin, I.; Hasan, M.; Hindmarsh, S.A.; Padrnos, J.D.; Edwards-Gayle, C.; Mathers, R.T.; Adams, D.J.; Sosso, G.C.; Gibson, M.I. Minimalistic ice recrystallisation inhibitors based on phenylalanine. *Chem. Commun.* **2022**, *58*, 7658–7661. [[CrossRef](#)] [[PubMed](#)]
32. Raymond, J.A.; DeVries, A.L. Adsorption inhibition as a mechanism of freezing resistance in polar fishes. *PNAS* **1977**, *74*, 2589–2593. [[CrossRef](#)] [[PubMed](#)]
33. Groot, C.C.M.; Meister, K.; DeVries, A.L.; Bakker, H.J. Dynamics of the Hydration Water of Antifreeze Glycoproteins. *J. Phys. Chem. Lett.* **2016**, *7*, 4836–4840. [[CrossRef](#)] [[PubMed](#)]
34. DeVries, A.L.; Komatsu, S.K.; Feeney, R.E. Chemical and Physical Properties of Freezing Point-depressing Glycoproteins from Antarctic Fishes. *J. Biol. Chem.* **1970**, *245*, 2901–2908. [[CrossRef](#)] [[PubMed](#)]
35. Harding, M.M.; Anderberg, P.I.; Haymet, A. ‘Antifreeze’ glycoproteins from polar fish. *Eur. J. Biochem.* **2003**, *270*, 1381–1392. [[CrossRef](#)] [[PubMed](#)]
36. Lin, Y.; Duman, J.G.; DeVries, A.L. Studies on the structure and activity of low molecular weight glycoproteins from an antarctic fish. *Biochem. Biophys. Res. Commun.* **1972**, *46*, 87–92. [[CrossRef](#)]
37. Budke, C.; Dreyer, A.; Jaeger, J.; Gimpel, K.; Berkemeier, T.; Bonin, A.S.; Nagel, L.; Plattner, C.; DeVries, A.L.; Sewald, N.; et al. Quantitative Efficacy Classification of Ice Recrystallization Inhibition Agents. *Cryst. Growth Des.* **2014**, *14*, 4285–4294. [[CrossRef](#)]
38. Furukawa, Y.; Nagashima, K.; Nakatsubo, S.-i.; Yoshizaki, I.; Tamaru, H.; Shimaoka, T.; Sone, T.; Yokoyama, E.; Zepeda, S.; Terasawa, T.; et al. Oscillations and accelerations of ice crystal growth rates in microgravity in presence of antifreeze glycoprotein impurity in supercooled water. *Sci. Rep.* **2017**, *7*, 43157. [[CrossRef](#)]
39. Deng, J.Z.; Apfelbaum, E.; Drori, R. Ice Growth Acceleration by Antifreeze Proteins Leads to Higher Thermal Hysteresis Activity. *J. Phys. Chem. B* **2020**, *124*, 11081–11088. [[CrossRef](#)]
40. Knight, C.; Driggers, E.; DeVries, A. Adsorption to ice of fish antifreeze glycopeptides 7 and 8. *Biophys. J.* **1993**, *64*, 252–259. [[CrossRef](#)]
41. Meister, K.; DeVries, A.L.; Bakker, H.J.; Drori, R. Antifreeze Glycoproteins Bind Irreversibly to Ice. *J. Am. Chem. Soc.* **2018**, *140*, 9365–9368. [[CrossRef](#)] [[PubMed](#)]
42. Lane, A.N.; Hays, L.M.; Tsvetkova, N.; Feeney, R.E.; Crowe, L.M.; Crowe, J.H. Comparison of the Solution Conformation and Dynamics of Antifreeze Glycoproteins from Antarctic Fish. *Biophys. J.* **2000**, *78*, 3195–3207. [[CrossRef](#)] [[PubMed](#)]
43. Lane, A.N.; Hays, L.M.; Crowe, L.M.; Crowe, J.H.; Feeney, R.E. Conformational and dynamic properties of a 14 residue antifreeze glycopeptide from Antarctic cod. *Protein Sci.* **1998**, *7*, 1555–1563. [[CrossRef](#)] [[PubMed](#)]
44. Franks, F.; Morris, E.R. Blood glycoprotein from antarctic fish possible conformational origin of antifreeze activity. *Biochim. Biophys. Acta* **1978**, *540*, 346–356. [[CrossRef](#)]
45. Mochizuki, K.; Molinero, V. Antifreeze Glycoproteins Bind Reversibly to Ice via Hydrophobic Groups. *J. Am. Chem. Soc.* **2018**, *140*, 4803–4811. [[CrossRef](#)]
46. Mallajosyula, S.S.; Vanommeslaeghe, K.; MacKerell, A.D. Perturbation of Long-Range Water Dynamics as the Mechanism for the Antifreeze Activity of Antifreeze Glycoprotein. *J. Phys. Chem. B* **2014**, *118*, 11696–11706. [[CrossRef](#)]
47. Giubertoni, G.; Meister, K.; DeVries, A.L.; Bakker, H.J. Determination of the Solution Structure of Antifreeze Glycoproteins Using Two-Dimensional Infrared Spectroscopy. *J. Phys. Chem. Lett.* **2019**, *10*, 352–357. [[CrossRef](#)]
48. Tsvetkova, N.M.; Phillips, B.L.; Krishnan, V.V.; Feeney, R.E.; Fink, W.H.; Crowe, J.H.; Risbud, S.H.; Tablin, F.; Yeh, Y. Dynamics of Antifreeze Glycoproteins in the Presence of Ice. *Biophys. J.* **2002**, *82*, 464–473. [[CrossRef](#)]

49. Urbańczyk, M.; Góra, J.; Latajka, R.; Sewald, N. Antifreeze glycopeptides: From structure and activity studies to current approaches in chemical synthesis. *Amino Acids* **2017**, *49*, 209–222. [[CrossRef](#)]
50. Sun, Y.; Giubertoni, G.; Bakker, H.J.; Liu, J.; Wagner, M.; Ng, D.Y.W.; Devries, A.L.; Meister, K. Disaccharide Residues are Required for Native Antifreeze Glycoprotein Activity. *Biomacromolecules* **2021**, *22*, 2595–2603. [[CrossRef](#)]
51. Czechura, P.; Tam, R.Y.; Dimitrijevic, E.; Murphy, A.V.; Ben, R.N. The Importance of Hydration for Inhibiting Ice Recrystallization with C-Linked Antifreeze Glycoproteins. *J. Am. Chem. Soc.* **2008**, *130*, 2928–2929. [[CrossRef](#)] [[PubMed](#)]
52. Eniade, A.; Purushotham, M.; Ben, R.N.; Wang, J.B.; Horwath, K. A serendipitous discovery of antifreeze protein-specific activity in C-linked antifreeze glycoprotein analogs. *Cell Biochem. Biophys.* **2003**, *38*, 115–124. [[CrossRef](#)]
53. Liu, S.; Ben, R.N. C-Linked Galactosyl Serine AFGP Analogues as Potent Recrystallization Inhibitors. *Org. Lett.* **2005**, *7*, 2385–2388. [[CrossRef](#)]
54. Tam, R.Y.; Rowley, C.N.; Petrov, I.; Zhang, T.; Afagh, N.A.; Woo, T.K.; Ben, R.N. Solution Conformation of C-Linked Antifreeze Glycoprotein Analogues and Modulation of Ice Recrystallization. *J. Am. Chem. Soc.* **2009**, *131*, 15745–15753. [[CrossRef](#)]
55. Zhang, W.; Liu, H.; Fu, H.; Shao, X.; Cai, W. Revealing the Mechanism of Irreversible Binding of Antifreeze Glycoproteins to Ice. *J. Phys. Chem. B* **2022**, *126*, 10637–10645. [[CrossRef](#)] [[PubMed](#)]
56. Bachtiger, F.; Congdon, T.R.; Stubbs, C.; Gibson, M.I.; Sosso, G.C. The atomistic details of the ice recrystallisation inhibition activity of PVA. *Nat. Commun.* **2021**, *12*, 1323. [[CrossRef](#)]
57. Naullage, P.M.; Molinero, V. Slow Propagation of Ice Binding Limits the Ice-Recrystallization Inhibition Efficiency of PVA and Other Flexible Polymers. *J. Am. Chem. Soc.* **2020**, *142*, 4356–4366. [[CrossRef](#)] [[PubMed](#)]
58. Naullage, P.M.; Lupi, L.; Molinero, V. Molecular Recognition of Ice by Fully Flexible Molecules. *J. Phys. Chem. C* **2017**, *121*, 26949–26957. [[CrossRef](#)]
59. Ding, Z.; Wang, C.; Zhou, B.; Su, M.; Yang, S.; Li, Y.; Qu, C.; Liu, H. Antifreezing Hydroxyl Monolayer of Small Molecules on a Nanogold Surface. *Nano Lett.* **2022**, *22*, 5307–5315. [[CrossRef](#)]
60. Tachibana, Y.; Fletcher, G.L.; Fujitani, N.; Tsuda, S.; Monde, K.; Nishimura, S.I. Antifreeze glycoproteins: Elucidation of the structural motifs that are essential for antifreeze activity. *Angew. Chem.* **2004**, *116*, 874–880. [[CrossRef](#)]
61. Hess, B.; Kutzner, C.; Van Der Spoel, D.; Lindahl, E. GROMACS 4: Algorithms for highly efficient, load-balanced, and scalable molecular simulation. *J. Chem. Theory Comput.* **2008**, *4*, 435–447. [[CrossRef](#)]
62. Abraham, M.J.; Murtola, T.; Schulz, R.; Páll, S.; Smith, J.C.; Hess, B.; Lindahl, E. GROMACS: High performance molecular simulations through multi-level parallelism from laptops to supercomputers. *SoftwareX* **2015**, *1*, 19–25. [[CrossRef](#)]
63. Robertson, M.J.; Tirado-Rives, J.; Jorgensen, W.L. Improved peptide and protein torsional energetics with the OPLS-AA force field. *J. Chem. Theory Comput.* **2015**, *11*, 3499–3509. [[CrossRef](#)] [[PubMed](#)]
64. Abascal, J.L.; Sanz, E.; Garcia Fernandez, R.; Vega, C. A potential model for the study of ices and amorphous water: TIP4P/Ice. *J. Chem. Phys.* **2005**, *122*, 234511. [[CrossRef](#)]
65. García Fernández, R.; Abascal, J.L.F.; Vega, C. The melting point of ice Ih for common water models calculated from direct coexistence of the solid-liquid interface. *J. Chem. Phys.* **2006**, *124*, 144506. [[CrossRef](#)] [[PubMed](#)]
66. Nosé, S. A unified formulation of the constant temperature molecular dynamics methods. *J. Chem. Phys.* **1984**, *81*, 511–519. [[CrossRef](#)]
67. Hoover, W.G. Canonical dynamics: Equilibrium phase-space distributions. *Phys. Rev. A* **1985**, *31*, 1695–1697. [[CrossRef](#)] [[PubMed](#)]
68. Parrinello, M.; Rahman, A. Polymorphic transitions in single crystals: A new molecular dynamics method. *J. Appl. Phys.* **1981**, *52*, 7182–7190. [[CrossRef](#)]
69. Bouvet, V.R.; Lorello, G.R.; Ben, R.N. Aggregation of antifreeze glycoprotein fraction 8 and its effect on antifreeze activity. *Biomacromolecules* **2006**, *7*, 565–571. [[CrossRef](#)]
70. Matsumoto, M.; Yagasaki, T.; Tanaka, H. GenIce: Hydrogen-Disordered Ice Generator. *J. Comput. Chem.* **2018**, *39*, 61–64. [[CrossRef](#)]
71. Nguyen, A.H.; Molinero, V. Identification of Clathrate Hydrates, Hexagonal Ice, Cubic Ice, and Liquid Water in Simulations: The CHILL+ Algorithm. *J. Phys. Chem. B* **2015**, *119*, 9369–9376. [[CrossRef](#)] [[PubMed](#)]
72. Xu, H.; Berne, B.J. Hydrogen-Bond Kinetics in the Solvation Shell of a Polypeptide. *J. Phys. Chem. B* **2001**, *105*, 11929–11932. [[CrossRef](#)]
73. Sugita, Y.; Okamoto, Y. Replica-exchange molecular dynamics method for protein folding. *Chem. Phys. Lett.* **1999**, *314*, 141–151. [[CrossRef](#)]
74. Patriksson, A.; van der Spoel, D. A temperature predictor for parallel tempering simulations. *PCCP* **2008**, *10*, 2073–2077. [[CrossRef](#)] [[PubMed](#)]
75. Torrie, G.M.; Valleau, J.P. Nonphysical sampling distributions in Monte Carlo free-energy estimation: Umbrella sampling. *J. Comput. Phys.* **1977**, *23*, 187–199. [[CrossRef](#)]
76. Lemkul, J.A.; Bevan, D.R. Assessing the Stability of Alzheimer’s Amyloid Protofibrils Using Molecular Dynamics. *J. Phys. Chem. B* **2010**, *114*, 1652–1660. [[CrossRef](#)]
77. Hub, J.S.; de Groot, B.L.; van der Spoel, D. g_wham—A Free Weighted Histogram Analysis Implementation Including Robust Error and Autocorrelation Estimates. *J. Chem. Theory Comput.* **2010**, *6*, 3713–3720. [[CrossRef](#)]
78. Kresse, G.; Hafner, J. Ab initio molecular dynamics for liquid metals. *Phys. Rev. B* **1993**, *47*, 558. [[CrossRef](#)]
79. Kresse, G.; Furthmüller, J. Efficient iterative schemes for ab initio total-energy calculations using a plane-wave basis set. *Phys. Rev. B* **1996**, *54*, 11169–11186. [[CrossRef](#)]

80. Kresse, G.; Joubert, D. From ultrasoft pseudopotentials to the projector augmented-wave method. *Phys. Rev. B* **1999**, *59*, 1758–1775. [[CrossRef](#)]
81. Blöchl, P.E. Projector augmented-wave method. *Phys. Rev. B* **1994**, *50*, 17953–17979. [[CrossRef](#)] [[PubMed](#)]
82. Perdew, J.P.; Burke, K.; Ernzerhof, M. Generalized Gradient Approximation Made Simple. *Phys. Rev. Lett.* **1996**, *77*, 3865–3868. [[CrossRef](#)] [[PubMed](#)]
83. Grimme, S.; Antony, J.; Ehrlich, S.; Krieg, H. A consistent and accurate ab initio parametrization of density functional dispersion correction (DFT-D) for the 94 elements H-Pu. *J. Chem. Phys.* **2010**, *132*, 154104. [[CrossRef](#)] [[PubMed](#)]
84. Monkhorst, H.J.; Pack, J.D. Special points for Brillouin-zone integrations. *Phys. Rev. B* **1976**, *13*, 5188–5192. [[CrossRef](#)]
85. Methfessel, M.; Paxton, A.T. High-precision sampling for Brillouin-zone integration in metals. *Phys. Rev. B* **1989**, *40*, 3616–3621. [[CrossRef](#)]
86. van der Spoel, D.; van Maaren, P.J.; Larsson, P.; Timneanu, N. Thermodynamics of Hydrogen Bonding in Hydrophilic and Hydrophobic Media. *J. Phys. Chem. B* **2006**, *110*, 4393–4398. [[CrossRef](#)]
87. Luzar, A.; Chandler, D. Hydrogen-bond kinetics in liquid water. *Nature* **1996**, *379*, 55–57. [[CrossRef](#)]
88. Sun, Z.; Liu, Q.; Qu, G.; Feng, Y.; Reetz, M.T. Utility of B-Factors in Protein Science: Interpreting Rigidity, Flexibility, and Internal Motion and Engineering Thermostability. *Chem. Rev.* **2019**, *119*, 1626–1665. [[CrossRef](#)]
89. Her, C.; Yeh, Y.; Krishnan, V.V. The Ensemble of Conformations of Antifreeze Glycoproteins (AFGP8): A Study Using Nuclear Magnetic Resonance Spectroscopy. *Biomolecules* **2019**, *9*, 235. [[CrossRef](#)]
90. Bush, C.A.; Feeney, R.E.; Osuga, D.T.; Ralapati, S.; Yeh, Y. Antifreeze glycoprotein. Conformational model based on vacuum ultraviolet circular dichroism data. *Int. J. Pept. Protein Res.* **1981**, *17*, 125–129. [[CrossRef](#)]
91. Wilkinson, B.L.; Stone, R.S.; Capicciotti, C.J.; Thaysen-Andersen, M.; Matthews, J.M.; Packer, N.H.; Ben, R.N.; Payne, R.J. Total synthesis of homogeneous antifreeze glycopeptides and glycoproteins. *Angew. Chem.* **2012**, *124*, 3666–3670. [[CrossRef](#)]
92. Hudait, A.; Qiu, Y.; Odendahl, N.; Molinero, V. Hydrogen-Bonding and Hydrophobic Groups Contribute Equally to the Binding of Hyperactive Antifreeze and Ice-Nucleating Proteins to Ice. *J. Am. Chem. Soc.* **2019**, *141*, 7887–7898. [[CrossRef](#)] [[PubMed](#)]
93. Qiu, Y.; Odendahl, N.; Hudait, A.; Mason, R.; Bertram, A.K.; Paesani, F.; DeMott, P.J.; Molinero, V. Ice Nucleation Efficiency of Hydroxylated Organic Surfaces Is Controlled by Their Structural Fluctuations and Mismatch to Ice. *J. Am. Chem. Soc.* **2017**, *139*, 3052–3064. [[CrossRef](#)]
94. Liu, X.; Geng, H.; Sheng, N.; Wang, J.; Shi, G. Suppressing ice growth by integrating the dual characteristics of antifreeze proteins into biomimetic two-dimensional graphene derivatives. *J. Mater. Chem. A* **2020**, *8*, 23555–23562. [[CrossRef](#)]
95. Ebbinghaus, S.; Meister, K.; Born, B.; DeVries, A.L.; Gruebele, M.; Havenith, M. Antifreeze Glycoprotein Activity Correlates with Long-Range Protein–Water Dynamics. *J. Am. Chem. Soc.* **2010**, *132*, 12210–12211. [[CrossRef](#)] [[PubMed](#)]
96. Pandey, P.; Mallajosyula, S.S. Elucidating the role of key structural motifs in antifreeze glycoproteins. *PCCP* **2019**, *21*, 3903–3917. [[CrossRef](#)]
97. Jin, T.; Long, F.Q.; Zhang, Q.; Zhuang, W. Site-specific water dynamics in the first hydration layer of an anti-freeze glyco-protein: A simulation study. *PCCP* **2022**, *24*, 21165–21177. [[CrossRef](#)]
98. Narayanan Krishnamoorthy, A.; Holm, C.; Smiatek, J. Local Water Dynamics around Antifreeze Protein Residues in the Presence of Osmolytes: The Importance of Hydroxyl and Disaccharide Groups. *J. Phys. Chem. B* **2014**, *118*, 11613–11621. [[CrossRef](#)]
99. Jin, S.; Yin, L.; Kong, B.; Wu, S.; He, Z.; Xue, H.; Liu, Z.; Cheng, Q.; Zhou, X.; Wang, J. Spreading fully at the ice-water interface is required for high ice recrystallization inhibition activity. *Sci. China Chem.* **2019**, *62*, 909–915. [[CrossRef](#)]

Disclaimer/Publisher’s Note: The statements, opinions and data contained in all publications are solely those of the individual author(s) and contributor(s) and not of MDPI and/or the editor(s). MDPI and/or the editor(s) disclaim responsibility for any injury to people or property resulting from any ideas, methods, instructions or products referred to in the content.